Chapter 7

Some Essential Issues and Outlook for Industrialization of Cu-III-VI_2 Thin-Film Solar Cells

Yijian Liu, Huey-Liang Hwang, Ying Wang,
Jun Zhang and Lexi Shao

Additional information is available at the end of the chapter

http://dx.doi.org/10.5772/intechopen.77023

Abstract

The concept and method of in-line sputtering and selenization become the industrial standard for Cu-III-VI_2 solar cell fabrication, but it is a difficult work to control and predict the electrical and optical performances, which are closely related to the chemical composition of the film. This chapter addresses the material design, device design, and process design using chemical compositions relating parameters. Compositional variation leads to change in the poisson equation, current equation and continuity equation governing the device design. To make the device design much realistic and meaningful, we have to build a model that relates the opto-electrical performance to the chemical composition of the film. The material and device structural parameters are input into the process simulation to give a complete process control parameters and method. We calculated neutral defect concentrations of non-stoichiometric $CuMSe_2$ (M-In, Ga) under the specific atomic chemical potential conditions. The electrical and optical performance has also been investigated for the development of full function analytical solar cell simulator. Module instability and their origins are listed. After that progress of CZTS (Cu_2ZnS_4) is briefed on the future work of CIGS ($CuInGaSe_2$). The future prospects regarding the development of CIGS thin-film solar cells (TFSCs) have also been discussed.

Keywords: Cu-III-VI_2, non-stoichiometric, material process and device design, module stability, progress of CZTS

1. Introduction

During past few decades the PV market has grown at a remarkable rate especially focused on the thin-film solar cells (TFSCs) and it is on their way to becoming a major source of electricity

production around the world. Although the research and development of CIGS are still in crucial phase due to low production yields, non-reproducibility, and non-uniformity over large area confronted during the industrialization and commercialization. Governing such issues, we published our first research paper in the year 2003 on "Steps toward industrialization of Cu-III-VI_2 thin film solar cells: A novel in-line concept" [1]. After that, the concept of in-line sputtering and selenization become international standard globally. From that time, dozens of CIGS manufacturing units established worldwide but rare claim successful in production due to difficulty in controlling the local chemical composition distribution of the film. Moreover, the production efficiency of large-area photovoltaic (PV) cells and panels varies in the wide range from 6 to 13%. During the decades of fast development of Cu-III-VI_2 thin film solar cells, much more research and industrial method were proposed. In this chapter, we will depict the principles and development of some essential issues for industrialization of Cu-III-VI_2 thin film solar cells.

In the year 2003, we published another research "Preliminary steps toward industrialization of Cu-III-VI_2 thin film solar cells: development of an intelligent design tool for non-stoichiometric photovoltaic materials" [1] pointing on the problem encountered during the commercialization. Over the years, many experimental and theoretical research works published in many journals focused on various subjects of problems and its solutions for CIGS TFSCs [2–9].

In 2013, we published one more research article "Steps toward removing some obstacles of industrialization of CIGS solar cells" [10]. This article pointing to the new concept of metal organic sputtering was used to tune and tailor the film compositions based on the programme material and device design. What shown in **Figure 1** is the method of our intelligence material and device design, describing the detailed calculation of the neutral defect concentrations of non-stoichiometric $CuInSe_2$, $CuGaSe_2$, and ZnO in specific atomic chemical potential conditions ($\mu x = 0$, X = Cu, In/Ga, Zn).

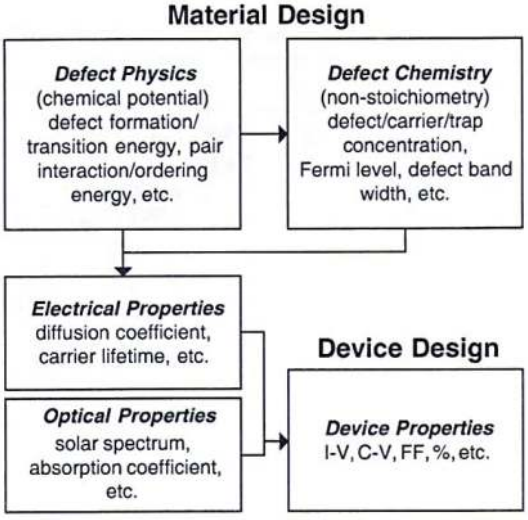

Figure 1. The scheme of our materials design and device design in which the electrical and device properties are optimized, and related to the process parameters such as, chemical potential and non-stoichiometry.

These main and key schemes of the intelligence design are the calculations of device and process design. The carrier concentration and the electrical properties of these materials with variable atomic constitutions are further calculated, which demonstrate the main functions of the CAD tool used [1, 10–13].

The present communication we have summed up the material design, device design, and process design to get deep knowledge on the chemical composition variation for obtaining the complete process control parameters. These designing tools will moderately help to overcome all the obstacles encountered during the industrialization of CIGS thin film solar cells. The future aspects of industrialization of CIGS thin film solar cells are also discussed.

2. Introduction on intelligence material design

2.1. Experimental data

We all know that Cu-III-VI_2 typically have a wide phase stability range, which extends a few atomic percents of the chemical composition of the thin-film, contract to III-V, and II-VI compounds. Shown in **Figure 2** is the chemical composition for a near-stoichiometric $CuInSe_2$. The variations in the $CuInSe_2$ film was detected using a transmission electron microscope (TEM) equipped with a field emission gun [10]. A similar result had also been reported for CIGS thin-film [11].

2.2. Theoretical data

In 2003, we published an example of the design tool for the non-stoichiometric compound using the concept of minimization of total free energy [1, 12, 13], which includes the configurational entropy, that defined as;

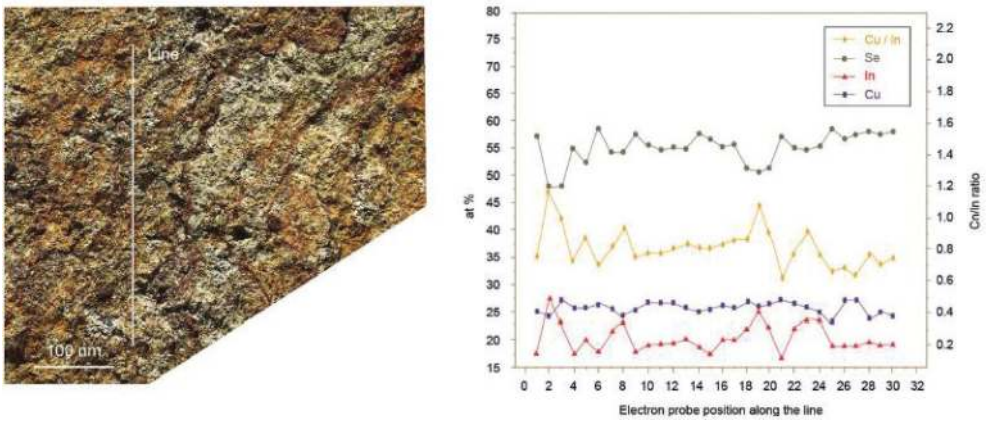

Figure 2. Chemical composition of a near-stoichiometric $CuInSe_2$ film measured consecutively by using an electron beam with a 3 nm probe size along a line marked on a TEM micrograph (left) and the plotted data (right) (corresponding to the data in **Table 1**).

	Cu(at%)	In(at%)	Se(at%)	Cu/In
Maximum	28.2	28.1	57.1	1.18
Minimum	17.2	22.6	47.9	0.62
Average	20.9	25.9	53.3	0.81
Standard deviation	2.73	1.37	2.80	0.12

Table 1. Chemical composition of a near-stoichiometric $CuInSe_2$ films.

$$G(T, \text{Crystal size}) = \Sigma n_i E_{fi} - TS_{config}, S_{config} = Kln\frac{N_{total}!}{\pi_j N_j!} \quad (1)$$

where n_i is the number of the ith defect, E_{fi} is the formation energy, S_{config} is the configurational entropy, T is the temperature, K is the Boltzmann constant, N is the total number of lattice sites, and Ni is the total number of defect sites of the i_{th} defect. We find the possible results for the co-existence of donors and acceptors in $CuMSe_2$ (M = In, Ga), which includes either the new defects produced through interaction or donor-acceptor pair/cluster formation.

Table 2 shows the defect formation energies and the defect transition levels. We also find the possible phases of $CuMSe_2$ resulted due to the compensated donor-acceptor pairs in different Cu concentration, for example, $Cu_1M_3Se_5$ phase is observed by 80% $Cu_1M_5Se_8$ and 20% $CuMSe_2$.

$CuInSe_2$		E_{for}	E_D/E_A	$CuGaSe_2$		E_{for}	E_D/E_A	ZnO		E_{for}	E_D/E_A
V_{Cu}	0	0.60	$E_v + 0.03$	V_{Cu}	0	0.66	$E_v + 0.01$	V_{Zn}	0	10.6	$E_v - 0.5$
	−1	0.63			−1	0.67			−1	10.1	$E_v + 0.0$
									−2	10.1	$(E_v - 0.25)$
V_{In}	0	30.4	$E_v + 0.17$	V_{Ga}	0	2.83	$E_v + 0.19$	V_O	+2	−3.0	$E_c + 1.2$
	−1	3.21	$E_v + 0.41$		−1	3.02	$E_v + 0.38$		+1	1.5	$E_c - 2.4$
	−2	3.62	$E_v + 0.67$		−2	3.40	$E_v + 0.66$		0	2.4	$(E_c - 0.6)$
	−3	4.29			−3	4.06					
V_{Se}	+2	1.12	$E_c - 0.1$	V_{Se}	+2	1.01	$E_c - 0.38$	Zn_i	+2	−2.3	$E_c + 1.1$
	+1	–			+1	–			+1	2.1	$E_c + 0.8$
	0	3.00			0	3.61			0	6.2	$(E_c + 0.95)$
Cu_i	+1	2.04	$E_c - 0.20$	Cu_i	+1	1.91	$E_c - 0.21$	O_i	0	9.7	$E_v + 0.7$
	0	2.88			0	3.38			−1	10.4	$E_v + 1.7$
									−2	12.1	$E_v + 1.2$
Cu_{In}	0	1.54	$E_v + 0.29$	Cu_{Ga}	0	1.41	$E_v + 0.29$	Zn_O	+2	0.4	$E_c + 1.5$
	−1	1.83	$E_v + 0.58$		−1	1.70	$E_v + 0.63$		+1	5.2	$E_c + 1.1$
	−2	2.41			−2	2.33			0	9.6	$(E_c + 1.3)$
In_{Cu}	+2	1.85	$E_c - 0.34$	Ga_{Cu}	+2	2.04	$E_c - 0.69$				
	+1	2.55	$E_c - 0.25$		+1	3.03	$E_c - 0.49$				
	0	3.34			0	4.22					
$V_{Se} + 2V_{Cu}$	0	3.63	–	$V_{Se} + 2V_{Cu}$	0	3.65	–				
$V_{Se} + Cu_{In}$	0	–	–	$V_{Se} + Cu_{Ga}$	0	–	–				
$2Cu_i + Cu_{In}$	0	3.11	–	$2Cui + Cu_{Ga}$	0	3.20	–				
$In_{Cu} + 2V_{Cu}$	0	0.33	–	$Ga_{Cu} + 2V_{Cu}$	0	0.74	–				

Table 2. The defect formation energies and defect transition levels used in our calculations [14].

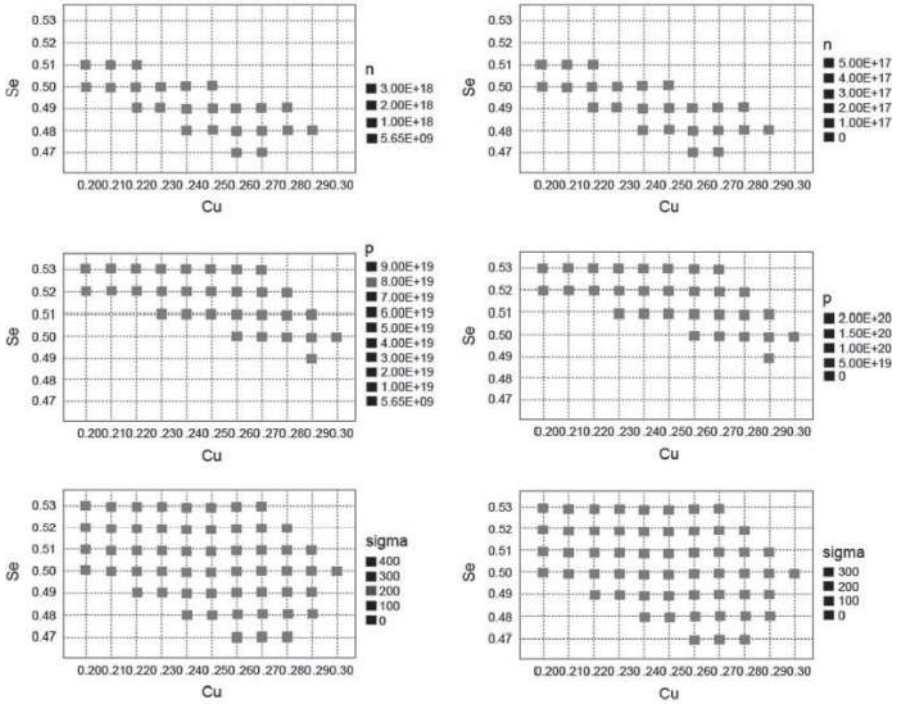

Figure 3. The calculated carrier concentration and electrical conductivity of $CuInSe_2$ (left) and $CuGaSe_2$ (right) at 300 K.

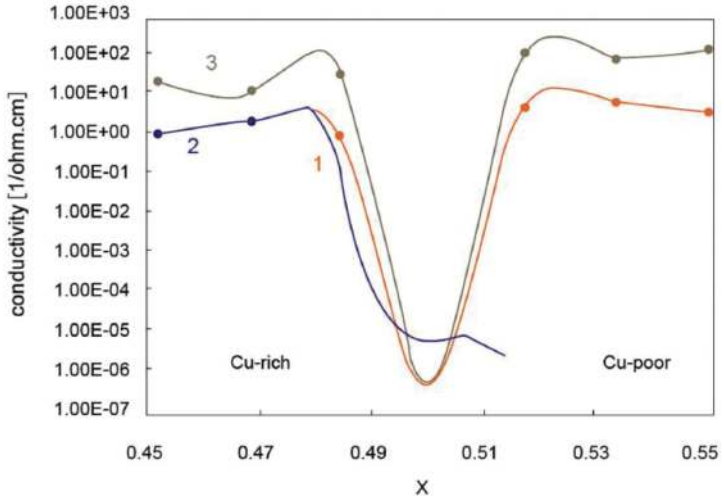

Figure 4. The measured conductivity of the $CuInSe_2$ thin-film along the Cu_2Se-In_2Se_3on-tie line with composition (Cu_2Se) $1-x(In_2Se_3)x$(line 1) and the calculated range (between line 2 and 3) near the Cu_2Se-In_2Se_3 tie line at 300 K.

To solve the charge neutrality equation, we require several parameters, such as the carrier concentrations, Femi level at a certain temperature and ionized/neutral defect concentrations. In **Figure 3**, the calculated carrier concentration and electrical conductivity of $CuInSe_2$ and $CuGaSe_2$ at 300 K are shown. Note that in **Figure 4**, the conductivity will increase first and then decrease down to the film composition from stoichiometry to Cu-poor, after that the conductivity is even lower than that of the stoichiometry.

3. Brief on the device design

The simulator SCADS 3.2 [15] has been widely accepted for numerical analysis of CIGS solar cell devices. In 2014, the 19% efficiency of the solar cell was simulated by Naoki Ashida et al. [16]. In this report, the 2 μm thick CIGS absorber layer was divided into two regions, such as low defect density region (front side) and high defect density region (back side).

We also developed an alternate full function (indoor, outdoor, and I-V, C-V) analytic solar cell simulator, in which the following (time-independent) device equations are considered.

a. The continuity equation

$$\mathrm{O} = -\frac{1}{\mathrm{q}}\frac{\mathrm{d}}{\mathrm{dx}}\tau_p + G_p - R_p, R_p = \frac{\Delta p}{\tau_h}, \Delta p = p_n - p_{no} \tag{2}$$

$$\mathrm{O} = -\frac{1}{\mathrm{q}}\frac{\mathrm{d}}{\mathrm{dx}}\tau_n + G_n - R_n, R_n = \frac{\Delta n}{\tau_e}, \Delta n = n_p - n_{po} \tag{3}$$

b. Transport equations

$$\tau_p = \mathrm{pq}\mu_p\,\mathrm{E} - \mathrm{q}D_p\frac{\mathrm{dp}}{\mathrm{dx}} \tag{4}$$

$$\tau_n = \mathrm{nq}\mu_n\,\mathrm{E} + \mathrm{q}D_n\frac{\mathrm{dn}}{\mathrm{dx}} \tag{5}$$

We have considered all the boundary conditions (n-QNR/SCR interface, front contact, p-QNR/SCR interface, and back contact), in which QNR stands for the quasi-neutral region and SCR stands for space charge region for a typical n-CdS/p-CIGS device structure. In results of our simulation, we show that the higher efficiency cells are distributed along the line from Cu:Se = 0.3:0.5 to the stoichiometric point and the line from Cu:Se = 0.21:0.52 to the stoichiometric point. What is shown in **Figure 5** is the comparison of the computed efficiencies with the national renewable energy laboratory (NREL) experimental data, where the device structures of these cells are $ZnO/CdS/CuInSe_2$. As to the higher efficiency cells, the atomic compositions are especially concentrated near Cu:Se = 0.22:0.51 or along the line from Cu:Se = 0.22:0.51 to the stoichiometric point.

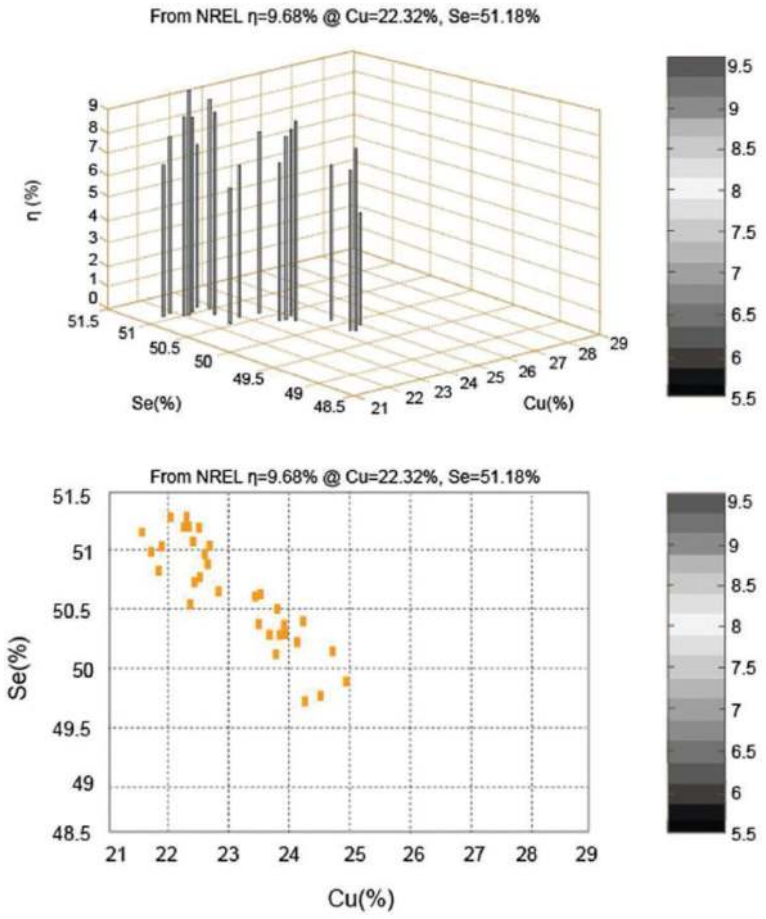

Figure 5. The comparison of the computed efficiencies as compared with NREL's database of ZnO/CdS/$CuInSe_2$ solar cells: (upper) 3D view, (lower) 2D view.

In the last decades, many studies on interface and surface compositional profile have been dealt with the advanced characterizations for the high-efficiency CIGS solar cells. A few examples are:

1. Conduction band profiles are changed by the three stage selenization [17].
2. Ordered defect compounds (ODC: $CuInSe_2$, $CuIn_3Se_5$, $CuIn_5Se_8$, etc.) resulted from $CuInSe_2$/CIGS solar cell studies, in which the X-ray photoelectron Spectroscopy (XPS) investigations depicted the depletion of Cu near the surface, and the theory as well experiments predicted ordered defect compound structured [18].
3. Shown in **Figure 6**, defect pairs ($2V_{cu}$ and In_{cu}) stabilizes the $CuInSe_2$ surface and band alignment gives hole barrier at the interface via the investigations by low energy electron

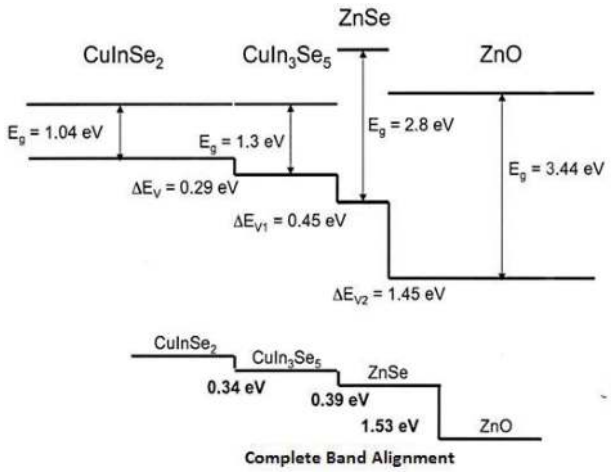

Figure 6. The complete band alignment includes the copper depletion at the interface.

diffraction (LEED), angular resolved ultraviolet photoelectron spectroscopy (ARUPS) and auger electron spectroscopy (AES) [14].

4. Secondary ion mass spectrometry (SIMS) depth profile of Cu, In, Ga, Se, Cd, and Na revealed the CdS/CIGS/ZnO diffusion phenomena as shown in **Figure 7** [19].

   Sample **Figure 7(a)** and **(b)** were obtained from the different origins, note that the difference in the Ga profile in the SIMS depth profiles are due to the different processes.

5. Defect in grains and grain boundaries [20].

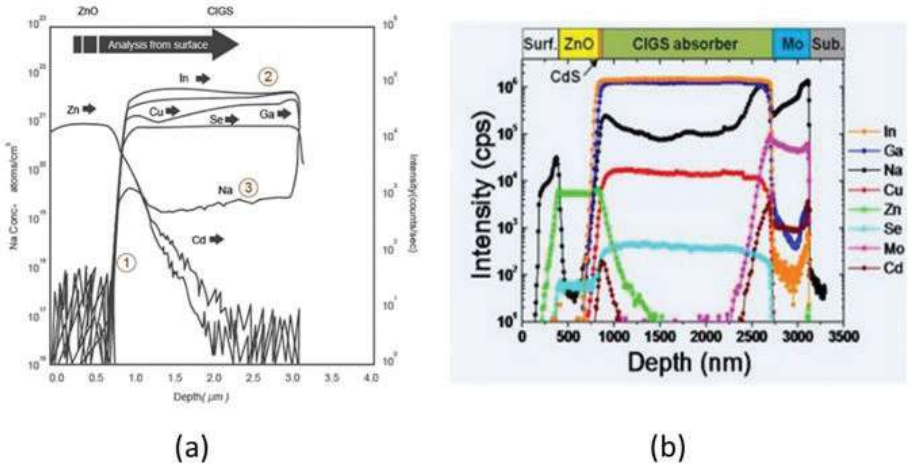

Figure 7. SIMS depth profile of Cu, In, Ga, Se, Cd, and Na. (1) CdS/CIGS and ZnO diffusion. (2) Cu, In, Ga, and Se depth profile. (3) Quantitative analysis of Na in CIGS.

The properties of the interfaces in semiconductor devices are critically dependent on the detailed atomic structure of the contact plane. Therefore, the model of the junction in chalcopyrite thin-films was simulated by the well-defined interface to classify the influence of grain boundaries, lateral inhomogeneity and chemical variations in compositions and their distributions across and aside from the contact planes. By X-ray photoelectron spectroscopy (XPS), ultra-violet photoelectron spectroscopy (UPS), Low energy electron diffraction (LEED), scanning tunneling microscopy (STM), and X-ray photoemission electron microscope (XPEEM), we can be obtain all these information using the modern analytic tools such as in-situ band alignment, band broadening, and chemical reacted interfaces. After that by experiments and incorporated with our material analysis we could determine their crystalline structure with high resolution for better accuracy and reproducibility obtained in the device design for the future industrial applications.

4. Brief on the process design

In sections above, the opto-electrical properties of the polycrystalline semiconductors are affected by structure and composition greatly.

In this section, the way of the poly-structure generation is better described through careful observation of the transfer procedures during the manufacturing process, which would be beneficial to know the deposited atoms final positions and the microstructures of the materials. The composition and the structures could be tuned based on controlling and modifying the process by adjusting the process parameters in order to obtain the desired opto-electrical properties.

We describe the better understanding of the way to generate poly-structure through careful observation of the particle transfer procedures during the manufacturing processes after knowing the final positions of the deposited atoms and the materials microstructures. On controlling and modifying the process, the composition as well structure can be tuned directly by varying the process parameters to acquire the desired opto-electrical properties.

The metallic grain structures are described by the original Thornton's zone model [21] according to the sputtering gas pressure and the substrate temperature. Since the high deposition rate, the magnetron sputtering process is most preferred for the industrial application. Also, the energy-dependent sputter yield is noted. Ellmer illustrates the inter-relationships between the process parameters (like substrate temperature and deposition rate) and the structural/optoelectrical properties in a new model [22]. However, the pressure (particles momentum) effect is not considered in this model.

4.1. Berg's model

The Berg's model is particularly utilized in the ZnO reactive sputtering. Basically, the surface coverage on the deposited film is just the composition of the film, but the composition is not easy to control since the system is unstable, where it requires the plasma diagnose sensor for feedback control. About the basic idea of the Berg's model [23, 24], the changes of the number of absorbed oxygen atoms per unit area Nx at the surfaces of the target is:

$$\frac{dN_T}{dt} = 2\alpha_t(1-\theta_1) - J/eS_N\theta_1 \tag{6}$$

At the substrate:

$$\frac{dN_S}{dt} = 2\alpha_C F(1-\theta_2) + \frac{J}{e}S_N\theta_1\frac{A_t}{A_C}(1-\theta_2) - \frac{J}{e}S_M(1-\theta_1)\frac{A_t}{A_C}\theta_2 \tag{7}$$

where αx is the sticking coefficients, Sx is sputtering yields, and θX is the coverage. What shown in **Figure 8** is the basic idea of Berg's model and in **Figure 9** is an example of the simulation result of the ZnO reactive sputtering system (θ_2 always <1). We also use the Berg's model to predict the composition of the compound thin-film. After that, we can also predict whether the operating point is stable. Therefore, we can investigate the time-dependent behavior of the reactive sputtering (**Figure 10**).

4.2. CISe RTP-the IEC's model

$$Cu_xIn_y + H_2Se\ (\text{or Se}). \tag{8}$$

After we finish the $CuInSe_2$ defect concentration calculations, we can apply the result to the model, which was developed by IEC [26] to predict the processing time under a certain process temperature.

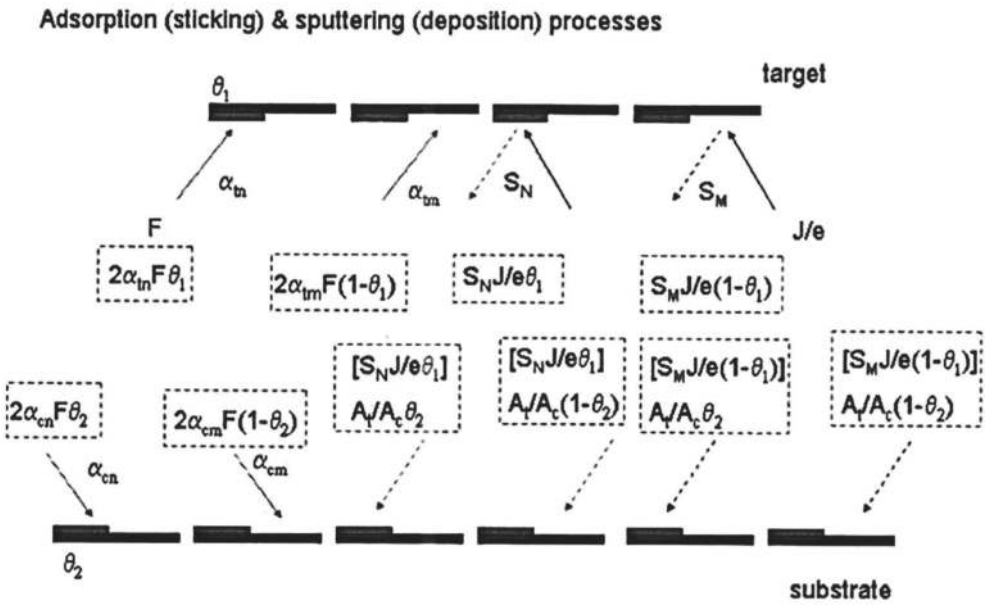

Figure 8. The basic idea of the Berg's model.

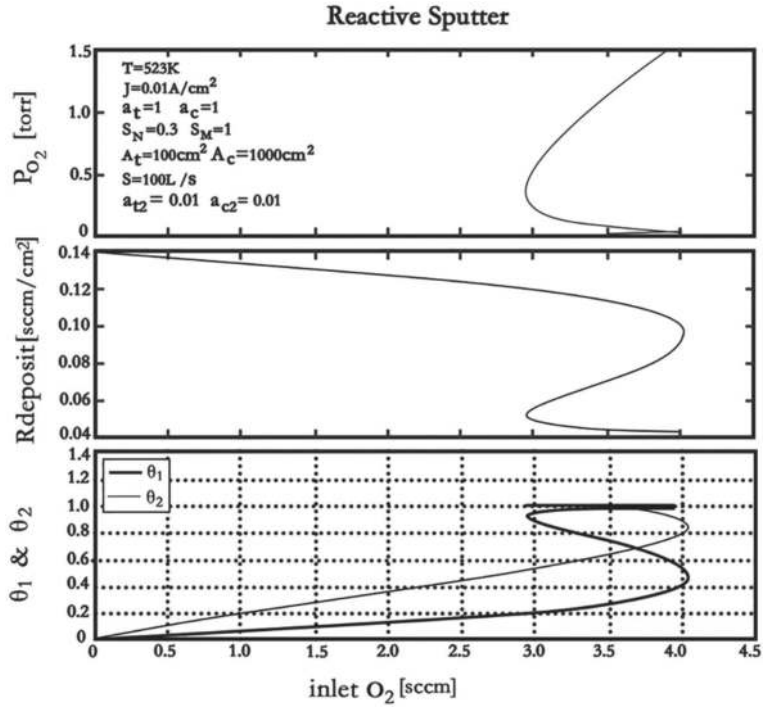

Figure 9. A simulation result of the ZnO reactive sputtering system [25].

For Cu In.

$$2In + Se \rightarrow In_2Se\ k_2 \tag{9}$$

$$In_2Se + Se \rightarrow 2InSe\ k_3 \tag{10}$$

$$2CuIn + 2Se \rightarrow Cu_2Se + In_2Se\ k_a \tag{11}$$

$$2InSe + Cu_2Se + Se \rightarrow 2CuInSe_2\ k_7 \tag{12}$$

where $K_i = K_{io}\exp\left(-\frac{E_{ai}}{RT}\right)$ and V=$\sum n_i x N_{Avo}\ x V_{unitcell}$, $n_{unitcell}$, is the film volume taken as a time-independent constant.

$n_i = [i]xV$ are the mole numbers, $n_{unitcell}$ is the number of pairs of the atoms in the unit cells. **Figure 10** shows an example of the Se or H_2Se RTP of Cu:In:Se = 0.24:0.25:0.51 CuxIny films at 450°C, μCu = 0, μIn = 0; the mole ratio of the constitute atoms (in the film) as functions of the processing time. (Film volume = (2.5 cm) 2 × 2 μm). In our non-stoichiometric case, the initial mole concentrations of Cu and in taken from our calculated data. Then, these were input to the CuxIny and in mole concentrations in order to solve the ordinary differential equation system.

Regarding building the non-stoichiometric structures, we build the XRD spectrum. The supercell values have been used to calculate the XRD spectrum of non-stoichiometric $CuInSe_2$

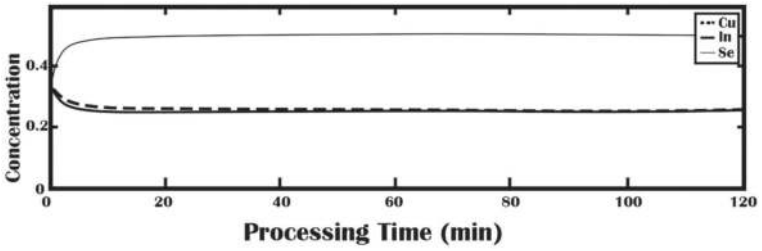

Figure 10. The Se or H_2Se RTP of Cu:In:Se = 0.24:0.25:0.51 CuxIny films at 450°C, μCu = 0, μIn = 0; the mole ratio of the constitute atoms (in the film) as functions of the processing time (120 min). (Film volume = (2.5 cm) 2 × 2 μm).

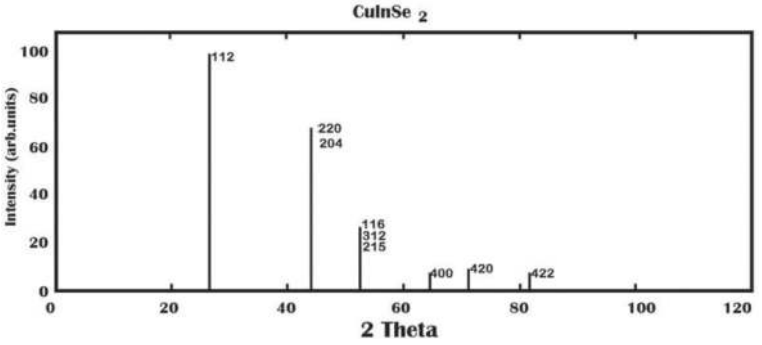

Figure 11. Simulated XRD spectra of non-stoichiometric CuInSe2; Cu:In:Se2 = 0.21:0.26:0.53.

and $CuGaSe_2$. In our work, the method described by Attia et al. [27] has been incorporated and only modify the structural factor by summing over all the atoms in the supercell. The defect site in each defect cells has been chosen randomly. We observed the presence of extra small peaks in the XRD spectrum, as shown in **Figure 11** [14].

Anomalous neutron diffraction scattering of synchrotron X-ray radiations gives more accurate data of composition distributions [28]. However, in-situ XRD is the most convenient tool for monitoring the deviations from the stoichiometric compositions. An incapability gap is indicated by the substantial increase in full width at half maximum (FWHM), in which the lattice constants depends on Ga/III and follow the Vegrad's law [29–31]. For industrial use for future process monitoring and control, more work should be done to make it more feasible to be used.

5. Some means to improve film composition control

When CIGS or other thin-films were fabricated, there will be chemical fluctuation-induced nano-domains. We developed a novel metal-organic sputtering (MO-sputtering) technique in our work, in which metal organic compound such as trimethygallium (TMGa) as the reactant was used during the reactive sputtering procedure. In **Figure 12**, the Ga/(Ga + In) ratio changes

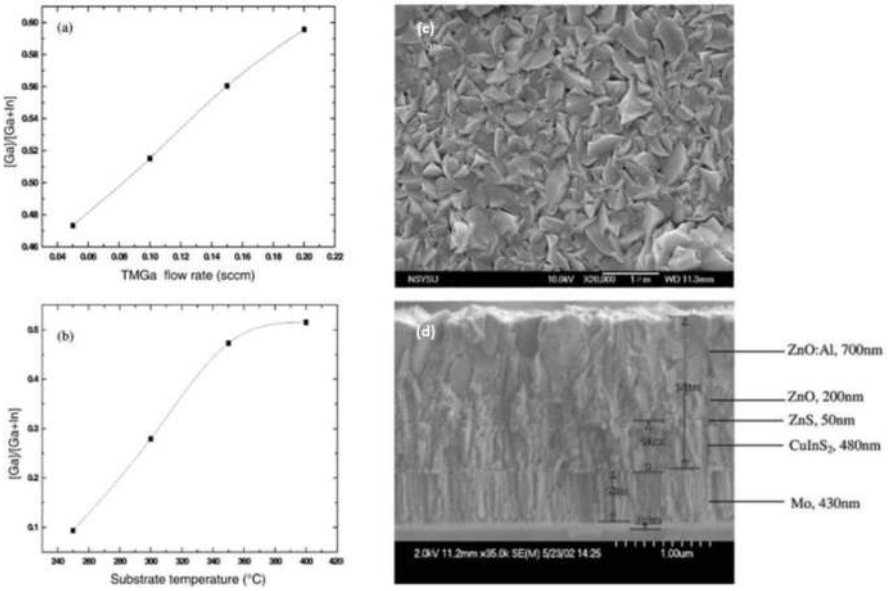

Figure 12. Preliminary result on the metal organic sputtering of CIGS PV. (a) Ga content as a function of TMGa flow rate, (b) the content of Ga as a function of substrate temperature, (c) plain view SEM image of the deposited CIGS film, and (d) cross-section.

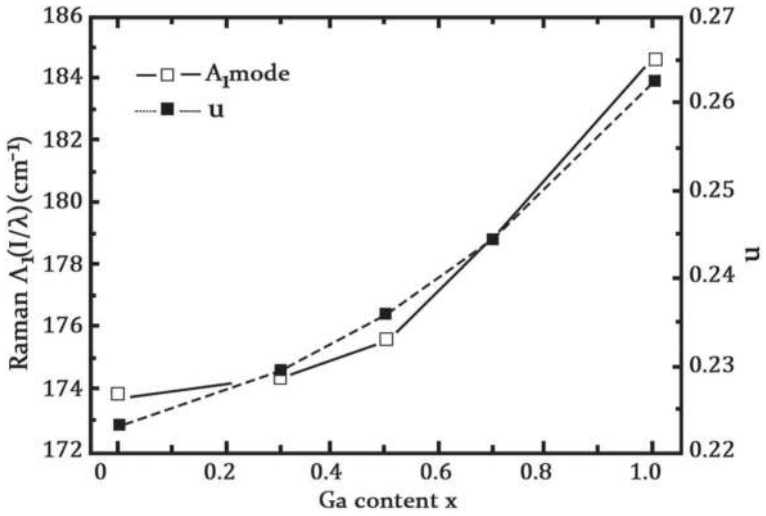

Figure 13. Room temperature Raman shift in $CuIn_1$–$xGaxSe_2$ thin-films of thickness 600 nm deposited on a glass substrate with a change in Ga content, the Raman peak shifted from 173.8 to 184.6 cm^{-1} in A1 mode and u is Se shift parameter. Reproduced with permission.

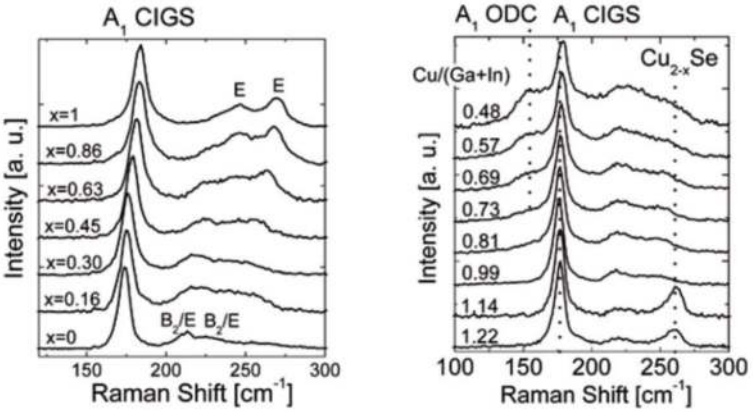

Figure 14. Micro-Raman spectroscopy results on the composition of thin-films.

as a function of TMGa flow rate and substrate temperature [1]. And the linear relationship of Ga/(Ga + In) with the TMGa flow rate to adjust the deposited film composition is particularly interesting. I could conclude from in **Figure 12** that the Raman shift as a function of the film composition change of Cu/(Ga + In) from the micro-Raman spectroscopy. It is clear that the micro-Raman shift is sensitive to the composition change of the CIGS thin-films. If we combine the use of Mo-Sputtering for the film growth and its feedback monitoring with the Raman shift, a means to better control the stoichiometry of thin-film might be provided during the manufacturing steps (**Figures 13** and **14**).

6. The stability of CIGS on an industrial scales

Degradation of modules at the moment, the highest conversion efficiency η of CIGS was 22.3% (Solar Frontier 2015) [32–38]. The three main parameters determining the cost competitiveness of electricity from PV panel is shown in **Figure 15**. The degradation rate per year is obtained by:

$$\text{Degradation } (\%) = \left(\frac{\eta_{\text{initial}} - \eta_{\text{final}}}{\eta_{\text{initial}} \times \text{Time}}\right) \times 100\%. \tag{13}$$

The time is given in year. **Table 3** shows the recently tested modules vary from very stable (No degradation after 7 years) to vulnerable to outdoor exposure.

Degradation depends on many parameters such as module production technologies, module type, production year, the orientation of the panel, climate, and installation location, as well as installation parameters like system voltage.

Generally, the investigation of degradation process in CIGS solar cells and modules is the complex and definite identification of failure mechanisms can be complicated.

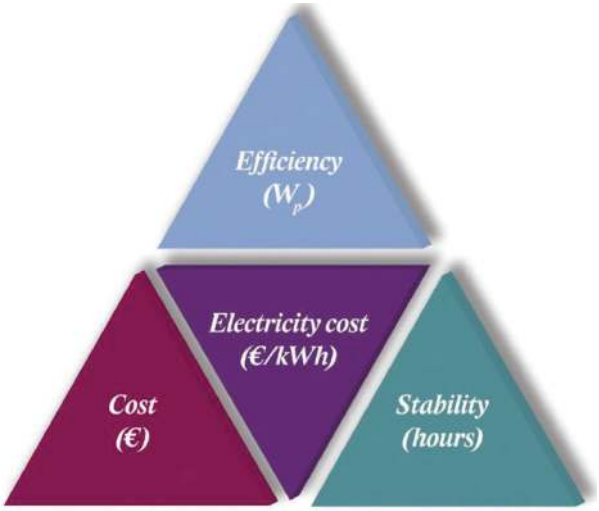

Figure 15. The three main parameters determining the cost competiveness of electricity from PV panels.

	Panel type/producer	Period	Location	Degradation rate (%/year)
Makrides et al. (2014), Phinikarides et al. (2015)	Würth WS11007/75	2006–2011	Nicosia, Cyprus	1.9 to 2.4
Dhere et al. (2011)		2005–2007	Florida, USA	4.5 to 5.1
Musikowski and Styczynski (2010)	Würth WS11007/75	2003–2010	Magdeburg, Germany	0
Del Cueto et al. (2008)		1990 (2002)–2008	Colorado, USA	0.2 to 2.3
Del Cueto et al. (2008)		2005–2008	Colorado, USA	2.5 to 4.7 (with bias)
Jordan and Kurtz (2011)	Shell Solar PowerMax Eclipse® 80-C	2006–2011	Colorado, USA	0
Jordan and Kurtz (2011)			Colorado, USA	0 to 3.7
Myers (2004)		2001 (10 months)	South-Africa	48
Myers (2004)		2001–2003	South-Africa	8.1
Niki et al. (2010)	ZSW	2003–2007	Widderstall, Germany	0.2
Ermer et al. (1990)	Siemens Solar	Until 1990 (17.5 months)	Colorado USA	4.1
Tarrant and Gay (2006)	Siemens Solar	1988–2006	Colorado USA	−0.2 to 1.7
Kushiya et al. (2006)	Showa Shell Sekiyu	2003–2006	Japan	0
Radue and Van Dyk (2009)		2007–2009 (13 months)	Port Elizabeth – South-Africa	−1.8 to 4.1

Table 3. Literature overview of degradation rates (%/year) of CIGS modules obtained from field tests at different locations.

Table 4 shows an overview of failure modules loading to CIGS module degradation and global categorization, when they are specific to CIGS or also observed for other thin-film modules. It was concluded that CIGS solar cells and modules are very sensitive to humidity. Furthermore, sensitivity to, for example, temperature (shocks), electrical bias, and illumination has been found, but the impacts of these loads are not necessarily detrimental.

Failure modes	CIGS specific	Impacted physical parameters	Possible failure mechanisms
1. Cell degradation			
A. Main junction: increase of recombination	Yes	Loss in FF, J_{sc} and V_{oc}	Diffusion of dopant, impurities, etc. + electromigration
B. Shunting	Yes	R_{shunt} decreases	Diffusion of metals, impurities, etc.
C. Series resistance increase by TCO and Mo degradation	Yes	R_s increases	Corrosion, diffusion
D. Delamination of back metal contact	Yes	J_{sc} decrease	Lamination stresses
2. Module degradation			
A. Interconnect resistance (ZnO: Al/Mo or Mo)	Yes	R_s increases	Corrosion, electromigration
B. Interconnect degradation – shunting: across isolation scribe	Yes	R_{sh} decreases	Corrosion, electromigration
C. Busbar failure	No	R_s increase or open circuit	Corrosion, electromigration
D. Solder joint	No	R_s increase or open circuit	Fatigue, coarsening (alloy segregation)
E. Encapsulation delamination	No	Loss in FF, J_{sc} and possible open circuit	Surface contamination, UV degradation, hydrolysis of silane/glass bond, warped glass, 'dinged' glass edges, thermal expansion mismatch
F. Encapsulation: loss or hermetic seal	No		
G. Encapsulation: glass breakage	No		
H. Encapsulation: Loss of high-potential isolation	No		

Table 4. Summary of failure as observed for CIGS.

7. Progress in thin-film solar cells (TFSCs) based on Cu_2ZnSnS_4 (CZTS)

CZTS is a material, which has been found in nature. **Figure 16** shows the content and the world trading price of the elements used in light absorbers CdTe, Cu_2ZnSnS_4, and $CuInSe_2$ for thin film solar cells [25, 39–49]. It shares similar structure which the chalcopyrite materials CuInS expect that half of the in is replaced with Zn and Sn. Crystallographically speaking, CZTS has two principal structures known as stannite-type and keasterit-type. The two structures are similar expect the different arrangement of Cu and Zn atoms. However, CZTS materials usually appear in keasterit phase because it is more stable.

Thermal dynamically compared to the stannite-type. The evolution of the power conversion efficiency of CZTS based solar cells is summarized in **Figure 17**.

The recorded power conversion efficiency of CZTSSe solar cells (12.6% reported in 2013) remains significantly than that of CIGSe (22.6%).

In order to improve the efficiency of CZTS based TFSCs, a deep research of CZTS based TFSCs and the fundamental properties of CZTS, particularly the nature of defects as well as their influence on the performance of CZTS materials is crucial. CZTS TFSCs, which have produced good efficiency normally, show Cu-poor/Zn-rich in composition. Therefore, secondly, phase should exist in the light absorber. It is necessary to identify those second phases and their defects in order to optimize the fabrication process to make CZTS thin-films with desired properties.

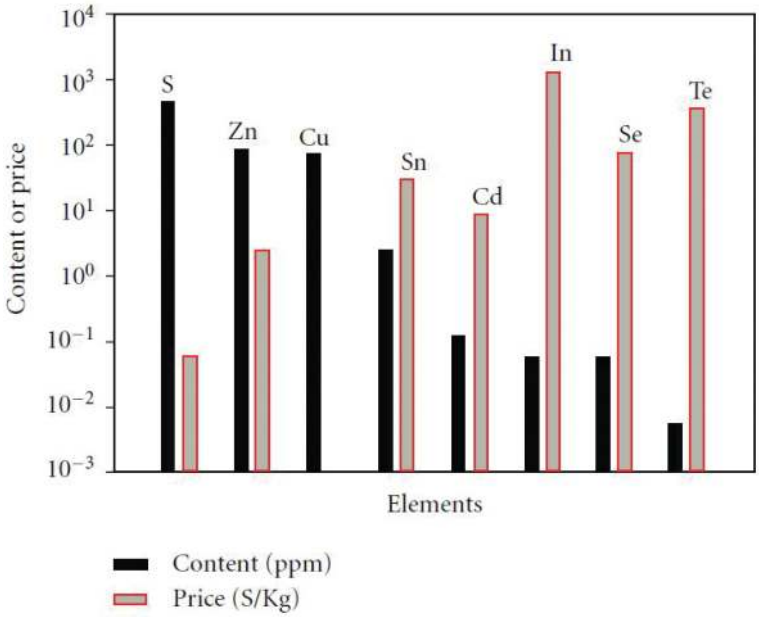

Figure 16. Content and the world trading price of the elements used in light absorbers CdTe, Cu_2ZnSnS_4, and $CuInSe_2$ for thin film solar cells.

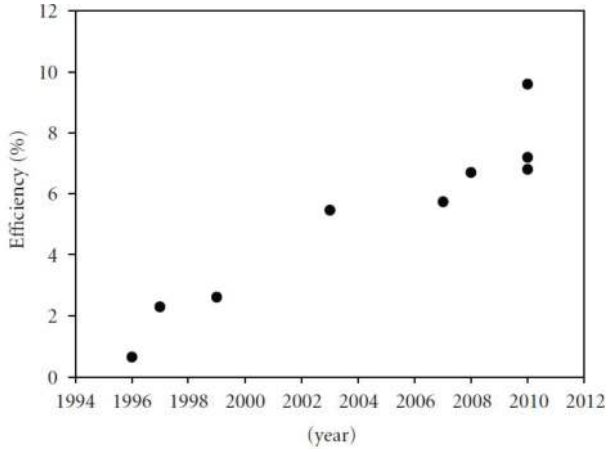

Figure 17. Evolution of the conversion efficiency of thin film solar cells using CZTS as light absorber layer.

8. Future aspects

Moreover, research institute NREL, USA and Fraunhofer ISE, Germany periodically publish the status reports on different stages of CIGS developments [49–52]. These reports greatly promote technology developments and industrialization of thin-film CIGS produces. Although, many challenges still lie ahead including optimization and control on the CIGS absorber film stoichiometry, interface, and film uniformity over large areas for the power module fabrication.

At presents, of monocrystalline and multicrystalline Si PV production, are dominant in the PV market, but the importance of TFSC will steadily rise in the coming decade. After that, in recent years the CIGS already win its own counterparts such as CdTe and a-Si (**Figure 18**) [53].

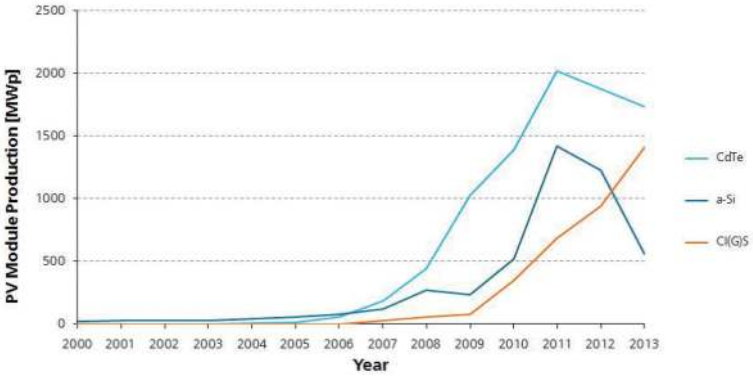

Figure 18. Thin-film technologies worldwide annual PV module production inMWp.

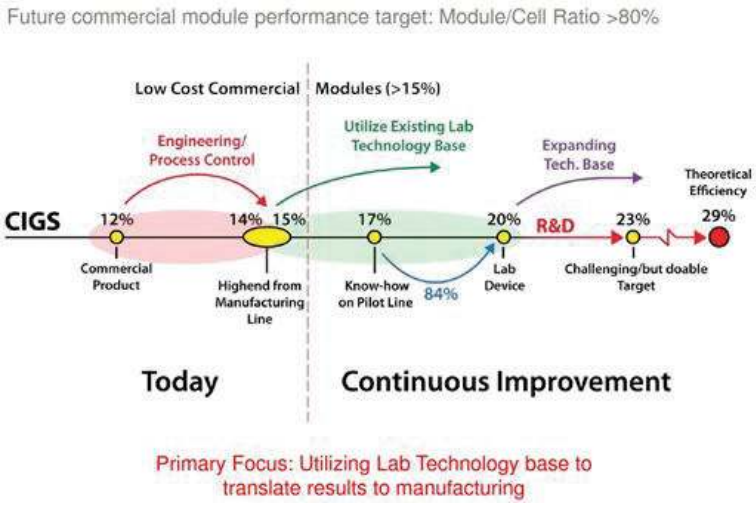

Figure 19. Closing the gap between laboratory cells and modules.

From the early report from NREL [54], it is greatly needed to develop continuous technologies to close the gap between laboratory cells and modules. And this is the purpose to develop science and technology to indicate the possibility to realize optimization and precise control of non-stoichiometric Cu-III-VI_2 compound in the future manufacturing (**Figure 19**).

9. Conclusions

In this chapter, we introduced the material designs on chemical compositions and compared some of the most important academic solar cell simulators. However, these simulators cannot load many files one by one and inevitably one analytic simulator favored especially for the non-stoichiometric PV materials, based on defect concentration of the CIGS alloy. This is the first phase to develop the comprehensive intelligent design (materials/devices/process). For industrial applications, much more refined detail work must be undertaken to further fulfill the need of PV cells for non-stoichiometric materials in a large area. For improving the process flow and performance of CIGS photovoltaic a fundamental improvement on the manufacturing technology and use of the concept of intelligent design are necessary. As CIGS PV technology matures to production on an industrial scale, the long-term stability becomes more important, which affects the cost the competitiveness of PV electricity and both the degradation rate of CIGS modules from a field test and their failure modes are listed. Moreover, the progress of thin film solar cells based on CZTS (Cu_2ZnSnS_4) is briefed, which shows future direction of material development of CIGS.

Acknowledgements

We gratefully acknowledge the financial support from ministry of science and technology of ROC.

Author details

Yijian Liu[1,2], Huey-Liang Hwang[1,2], Ying Wang[2]*, Jun Zhang[3] and Lexi Shao[3]

*Address all correspondence to: yingwang@sjtu.edu.cn

1 National Tsing Hua University, Hsinchu, Taiwan ROC

2 Shanghai Jiao Tong University, Shanghai, China

3 Lingnan Normal University, Zhanjiang, China

References

[1] Chang HH, Ueng HY, Hwang HL. Preliminary steps toward industrialization of Cu-III-VI_2 thin-film solar cells: development of an intelligent design tool for non-stoichiometric PV materials. Journal of Physics & Chemistry of Solids. 2003;**64**(9):2047-2053

[2] Jackson P, Hariskos D, Lotter E, et al. New world record efficiency for Cu(In,Ga)Se_2 thin-film solar cells beyond 20%. Progress in Photovoltaics Research & Applications. 2011; **19**(7):894-897

[3] Candelise C, Speirs JF, Gross RJK. Materials availability for thin film (TF) PV technologies development: A real concern? Renewable & Sustainable Energy Reviews. 2011;**15**(9):4972-4981

[4] Dhere NG. Scale-up issues of CIGS thin film PV modules. Solar Energy Materials & Solar Cells. 2011;**95**(1):277-280

[5] Panthani MG, Akhavan V, Goodfellow B. Synthesis of $CuInS_2$, $CuInSe_2$, and Cu(In_xGa_{1-x})Se_2 (CIGS) Nanocrystal "Inks" for printable photovoltaics. Journal of the American Chemical Society. 2008;**130**(49):16770

[6] Guo Q, Ford GM, Yang WC, et al. Fabrication of 7.2% efficient CZTSSe solar cells using CZTS nanocrystals. Journal of the American Chemical Society. 2010;**132**(49):17384-17386

[7] Todorov TK, Gunawan O, Gokmen T, et al. Solution-processed Cu(In,Ga)$(S,Se)_2$, absorber yielding a 15.2% efficient solar cell. Progress in Photovoltaics Research & Applications. 2013;**21**(1):82-87

[8] Chung CH, Song TB, Bob B, et al. Silver nanowire composite window layers for fully solution-deposited thin-film photovoltaic devices. Advanced Materials. 2012;**24**(40):5499-5504

[9] Akhavan VA, Goodfellow BW, Panthani MG, et al. Colloidal CIGS and CZTS nanocrystals: A precursor route to printed photovoltaics. Journal of Solid State Chemistry. 2012;**189**(24):2-12

[10] Hwang HL, Tseng BH, Jagadhamma LA, et al. Steps towards removing some obstacles of industrialization of CIGS solar cells. Physica Status Solidi. 2013;**10**(7–8):1046-1049

[11] Yan Y, Noufi R, Jones KM, et al. Chemical fluctuation-induced nanodomains in cu(in,Ga)Se_2 films[J]. Applied Physics Letters. 2005;**87**(12):225

[12] Chang HH, Ueng HY, Hwang HL. Preliminary steps toward industrialization of Cu-III-VI_2 thin-film solar cells: Development of an intelligent design tool for non-stoichiometric photovoltaic materials. Journal of Physics & Chemistry of Solids. 2003;**64**(9):2047-2053

[13] Chang HH, Ueng HY, Zhong TX. New perspectives of defect physics and defect chemistry for copper ternary chalcopyrite semiconductors. Japanese Journal of Applied Physics. 2000;**39**(S1):399

[14] Wei SH, Zunger A. Calculated natural band offsets of all II–VI and III–V semiconductors: Chemical trends and the role of cation d orbitals. Applied Physics Letters. 1998;**72**(16): 2011-2013

[15] Burgelman M, Nollet P, Degrave S. Modelling polycrystalline semiconductor solar cells. Thin Solid Films. 2000;**361**(99):527-532

[16] Ashida N, Murata M, Hironiwa D, et al. Numerical analysis of Cu(In,Ga)Se_2 solar cells with high defect density layer at back side of absorber. Physica Status Solidi. 2015;**12**(6): 638-642

[17] Wada T, Maeda T. Characteristics of chemical bonds in $CuInSe_2$, and its thin film fabrication processes used to fabricate solar cells (<Special Issue> Crystals Science and Technology of Solar Cells Materials -Concentrated on Crystal Growth-). 2009;**36**(4):282-289

[18] Zhang SB, Wei SH, Zunger A, et al. Defect physics of the $CuInSe_2$, chalcopyrite semiconductor. Physical Review B, Condensed Matter. 1998;**57**(16):9642-9656

[19] Yamada T. Lecture Notes on SIMS Data Presented at 19th International Conference on Ternary and Multinary Compounds; Niigata; September 2014

[20] Pettenkofer C. Energy Converting Interfaces Studied by Synchrotron Radiation. Berlin: Helmholtz-Zentrum. (pettenkofer@helmholtz-berlin.de)

[21] Thornton JA. The microstructure of sputter-deposited coatings molecular dynamics modeling of microstructure and stresses in sputter-deposited thin films. Journal of Vacuum Science & Technology. 1986;**A4**:3059

[22] Ellmer K. Magnetron sputtering of transparent conductive zinc oxide: relation between the sputtering parameters and the electronic properties. Journal of Physics D: Applied Physics. 2000;**33**(4):R17-R32(16)

[23] Berg S, Blom H, Larsson T, et al. Modeling of reactive sputtering of compound materials. Journal of Vacuum Science & Technology A Vacuum Surfaces & Films. 2015;**5**(2):202-207

[24] Berg S, Nyberg T, Blom H-O, Nender C. In: Glocker DA, Shah SI, editors. Handbook of Thin Film Process Technology. Bristol, UK: IOP Publishing; 1995

[25] Ito K, Nakazawa T. Electrical and optical properties of stannite-type quaternary semiconductor thin films. Japanese Journal of Applied Physics. 1988;**27**(11):2094-2097

[26] Orbey N, Norsworthy G, Birkmire RW, et al. Reaction analysis of the formation of $CuInSe_2$, films in a physical vapor deposition reactor. Progress in Photovoltaics Research & Applications. 1998;**6**(2):79-86

[27] Attia AA, Lachab M, Harsono S, et al. Crystal structure and composition of polycrystalline $CuInSe_2$[J]. Renewable Energy. 1995;**6**(5-6):559-565

[28] Schorr S. The crystal structure of kesterite type compounds: A neutron and X-ray diffraction study. Solar Energy Materials & Solar Cells. 2011;**95**(6):1482-1488

[29] Stephan C, Schorr S, Tovar M, et al. Comprehensive insights into point defect and defect cluster formation in $CuInSe_2$. Applied Physics Letters. 2011;**98**(9):668

[30] Schnohr CS, Kämmer H, Stephan C, et al. Atomic-scale structure and band-gap bowing in $Cu(In,Ga)Se_2$. Physical Review B. 2012;**103**(8):894-R1713

[31] Schorr S, Gurieva G. ICTMC-19; Niigata, Abstract Thu-I-2A; 2014

[32] Theelen M, Foster C, Barreau N, Steijvers H, Vroon Z, Zeman M. Influence of atmospheric species water, oxygen, nitrogen and carbon dioxide on the degradation of CIGS solar cells. Solar Energy Materials & Solar Cells. 2015;**141**:49-56

[33] Theelen M, Harel S, Verschuren M, et al. Influence of Mo/$MoSe_2$, microstructure on the damp heat stability of the Cu(In,Ga)Se_2, back contact molybdenum[J]. Thin Solid Films. 2016;**612**:381-392

[34] Thompson C, Hegedus S, Carcia P, Scott McLean R. The effects of device geometry and TCO/buffer layers on damp heat accelerated lifetime testing of Cu(In,Ga)Se_2 solar cells. IEEE Journal of Photovoltaics. 2013;**3**(1):494-499

[35] Walter T, Herberholz R, Muller C, Schock H. Determination of defect distributions from admittance measurements and application to CIGS-based heterojunctions. Journal of Applied Physics. 1996;**80**(8):4411-4420

[36] Wennerberg J, Kessler J, Stolt L. Design of grided Cu(In,Ga)Se2 thin-film PV modules. Solar Energy Materials & Solar Cells. 2001;**67**:59-65

[37] Wennerberg J. Design and stability of Cu(In, Ga)Se2-based solar cell modules. Acta Universitatis Upsaliensis. Comprehensive Summaries of Uppsala Dissertations from the Faculty of Science and Technology. Uppsala. 2002;**683**:91

[38] Wennerberg J, Kessler J, Stolt L. Cu(In,Ga)Se_2-based thin-film photovoltaic modules optimized for long-term performance. Solar Energy Materials & Solar Cells. 2003;**75**:47-55

[39] Olekseyuk ID, Dudchak IV, Piskach LV. Phase equilibria in the Cu_2S-ZnS-SnS_2 system. Journal of Alloys and Compounds. 2004;**368**:135-143

[40] Friedlmeier TM, Wieser N, Walter T, Dittrich H, Schock HW. Heterojuncitons based on Cu2ZnSnS4 and Cu2ZnSnSe4 thin films. In: Proceedings of the 14th European Conference of Photovoltaic Science and Engineering and Exhibition; Bedford; 1997. p. 1242

[41] Katagiri H, Saitoh K, Washio T, et al. Development of thin film solar cell based on Cu_2ZnSnS_4, thin films. Solar Energy Materials & Solar Cells. 2001;**65**(1):141-148

[42] Jafarov MA. Cu_2ZnSnS_4 thin film solar cells. Thin Solid Films. 2005;**480–481**(3):426-432

[43] Katagiri H, Jimbo K, Maw WS, et al. Development of CZTS-based thin film solar cells. Thin Solid Films. 2009;**517**(7):2455-2460

[44] Seol JS, Lee SY, Lee JC. Electrical and optical properties of Cu_2ZnSnS_4 thin films prepared by rf magnetron sputtering process. Solar Energy Materials & Solar Cells. 2003;**75**(1):155-162

[45] Liu F, Zhang K, Lai Y, et al. Growth and characterization of Cu_2ZnSnS_4 thin films by DC reactive magnetron sputtering for photovoltaic applications. Combustion & Flame. 2010; **13**(11):161-170

[46] Friedlmeier TM, Dittrich H, Schock HW. Growth and characterization of Cu_2ZnSnS_4 and $Cu_2ZnSnSe_4$ thin films for photovoltaic applications. Ternary and Multinary Compounds. 1998;**152**:345-348

[47] Kamoun N, Bouzouita H, Rezig B. Fabrication and characterization of Cu_2ZnSnS_4 thin films deposited by spray pyrolysis technique. Thin Solid Films. 2007;**515**:5949-5952

[48] Chen SY, Yang JH, Gong XG, Walsh A, Wei SH. Intrinsic point defects and complexes in the quaternary kesterite semiconductor Cu_2ZnSnS_4. Physical Review B. 2010;**81**:24

[49] Hamri EE, Meddah M, Boulkadat L, Elfanaoui A, Bouabid K, Nya M, Portier X, Ihlal A. Studies of non-vacuum processing of Cu-Chalcogenide thin films. Journal of Nanoscience and Nanotechnology. 2012;**12**(8):6800-6803

[50] Delahay AE, Bruns J, Rupper A, Akhtor M, Chen L, Kiss ZJ. Thin Film CIGS Photovoltaic Technology. Annual Technical Report Phase II 16 April 1999-15 April 2000

[51] Noufi R. High Efficiency CdTe and CIGS Thin Film Solar Cells! Highlights of the Technologies Challenges, presented at the 2006 IEEE 4th World Conference on Photovoltaic Energy Conversion (WCPEC-4); May 7-12, 2006; Waikyloa

[52] Ullal HS. Polycrystalline Thin-Film Solar Cell Technologies, presented at the 18th International Photovoltaic Science and Engineering Conference and Exhibition; January 19-23; Kolkata; 2009

[53] Fraunhoffer Institute for Solar Energy Systems ISE Photovoltaic Report. Freiburg 24 October 2014

[54] Noufi R. CIGS PV Technology: Challenges, Opportunities and Potential, NCPV, NREL, US; February, 2013